TRI-SERVICE 2007 CORROSION CONFERENCE
ARMY • NAVY • AIR FORCE • MARINES • COAST GUARD • NASA

High Silicone Content Barrier Coatings for Corrosion Protection of Metals

Atul Tiwari and L.H. Hihara
Hawaii Corrosion Laboratory, Department of Mechanical Engineering,
University of Hawaii at Manoa, Honolulu 96822
Email: tiwari@hawaii.edu

ABSTRACT

Organic-inorganic, ceramic-polymer hybrid (i.e., ceramer) materials are largely being used as barrier coatings for the corrosion protection of metals. Although these hybrid ceramers possess excellent environmental stability, their long term usage in aggressive climatic conditions is still questionable. Free volume associated with these hybrid coatings often provides percolation pathways for the ions and electrolyte to reach the substrate material leading to corrosion initiation. We have recently developed a novel coating formulation consisting of high silicone content, which significantly reduces the free volume in the coating. The hydrocarbon content was optimized to impart planarization characteristics to the solid coating. This coating precursor also etches the oxide layer of the metal surface to reveal the hydroxyl functionality for the reaction. Specialty chemicals present in the coating composition provides in-situ buffering action to control the pH of the reaction medium. Titanium oxide nanoparticles embedded in the backbone of the coating structure enhances scratch and UV resistance. In this communication, we investigate the barrier strength of this high-silicone coating. Fourier transformation infra-red spectroscopy and Raman spectroscopy was used to confirm the macromolecular structure of the precursor as well as the cured coating. Thermal stability of the solid coating was assessed by thermogravimetry, and the mechanical strength was evaluated utilizing the nanoindentation technique. Surface morphology associated with the condensed coating was studied using scanning electron microscopy and atomic force microscopy. A comparison between coated and uncoated metal coupons exposed to outdoor test sites and laboratory corrosion experiments are reported.

Keywords: Ceramer, Coatings, Characterization, Corrosion, Microscopy, Nanoindentation, Silicones

INTRODUCTION

Organic coatings are flexible and used throughout industry, but they are susceptible to in-diffusion of moisture due to their microporous structure, and also degrade in the presence of solar radiation. Inorganic coatings with dense ceramic-like structures can be made relatively impervious and resistant to solar degradation. They can also be applied to substrates that have anchor points upon which the coating can adhere. A major short coming, however, is their brittleness and susceptibility to cracking on flexible substrates.

Development of inorganic-organic hybrid ceramer coatings that can resist the in-diffusion of moisture, possess resistance to solar radiation, and have suitable flexibility is critical to the field of corrosion prevention. In this communication, we give an account of the various stages involved in the development of a high-silicone ceramer coating that can be used as an effective barrier against corrosion on aluminum.

BACKGROUND

In order for a coating to adhere to a substrate, specialty functional groups in the coating must form permanent bonds with the substrate; most of such functionalities involve hydrocarbons in their molecular structure. Introduction of hydrocarbon chains in the coating formulation often leads to a semiporous microstructure that is prone to premature failure. Reduction or possible elimination of hydrocarbons from the coating structure is often desired for synthesizing impervious coating. Very little work has been done in this area due to a scarcity of methods available for the production of a reactive coating without the use of hydrocarbons in the formulation. This section describes research done in the last few years in the field of silicone-containing ceramer coatings.

Pena-Alonso et al. [1] developed a hybrid material by combining tetraethoxysilane, polydimethylsiloxane, and tetrabutylorthotitanate in isopropyl alcohol as a solvent and hydrocholoric acid as a catalyst. They measured surface physical and chemical properties of the hybrid material using inverse gas chromatography in conjunction with nitrogen adsorption, mercury porosimetry, and Fourier transformation infra-red spectroscopy. They found that the micropore and misopore volume decreased, while the macropore size increased in correlation with the increase in tetrabutylorthotitanate content in the hybrid material.

Etienne-Calas [2] et al. studied the fracture mechanism of an inorganic-organic hybrid coating on substrates using the nanoindentation technique. At lower loads, they determined coating hardness and modulus values from indentation curves. At higher load values, propagation of cracks was used to determine the coating toughness, residual stress and interface toughness, while energetic analysis was used to study chipping and delamination in the coating. They found that mechanical properties of the coatings were influenced by the rapid diffusion of the sodium ions into the coating from the glass substrate.

Wu et al. [3] formulated a transparent hydrophobic coating by modifying a mixture of polydimethylsiloxane and ethylacetoacetate with titaniumtetraisopropoxide. Contact angles were modified by changing the concentration of polydimethylsiloxane in coating formulations. They found that the maximum water contact angle on the coating surface was achieved at 50 vol% of polydimethylsiloxane. The coating hardness increased as the silica filler content and curing temperature increased. The coating hardness, however, was inversely proportional to the polydimethylsiloxane concentration.

Al-Juhani et al. [4] reported on antifouling coatings. Their work incorporated benzoic acid and sodium benzoate in end-group terminated polysiloxane. They found that benzoic acid formed large crystals in the matrix that can leach out of the coating. The coating containing sodium benzoate exhibited enhanced antibacterial behavior as compared to the control sample coating of silicone.

Zucchi et al. [5] studied the effect of cerium salt, 3-mercapto-propyl-trimethoxysilane, and octadecyl-trimethoxysilane treatment on magnesium alloys. They found that treating the alloy with cerium salt does not improve the alloy's corrosion resistance. Treating the alloy with hydroalcoholic solution or octadecyl-trimethoxysilane was effective against corrosive media, while treating it with 3-mercapto-propyl-trimethoxysilane had less effect as compared to the former case.

Kumar et al. [6] formulated a siliconized epoxy interpenetrating coating system using epoxy resin as the base, hydroxyterminated polydimethylsiloxane as a modifier, γ-aminopropyltrimethoxysilane as a crosslinker, and dibutyltindilaurate as a catalyst. Polyamidoamine, aromatic amine adducts, and phosphorous containing diamines were used as catalysts. They evaluated corrosion and fouling resistance behavior of controlled epoxy and siliconized epoxy coatings with potentiodynamic polarization, electrochemical impedance spectroscopy, salt spray, and antifouling tests. They found that siliconized epoxy coatings exhibited a lower corrosion current and higher paint film resistance than a pure epoxy coating. They concluded that epoxy coatings modified with silicone/phosphorous have improved corrosion resistance also preventing the adherence and settling of marine organisms on steel.

Merabedini et al. [7] compared tin-based self-polishing tin-acrylic copolymer coatings with a silicone fouling-release coating for wettability and surface roughness. Drag measurements suggested that the frictional resistance of the silicone coating is lower than that of tin-acrylic copolymer coatings. Also, since the silicone coating increases surface hydrophobicity, it is less prone to adhesion of fouling organisms.

Trabelsi et al. [8] studied the self-healing capability of cerium nitrate doped (triethoxysilylpropyl)-tetrasulfide silane solutions as a pretreatment for galvanized steel. They proposed that precipitation of cerium oxides and hydroxides in anodic areas inhibit the transfer of electrons from anodic to cathodic sites. It is due to this hindrance mechanism that cerium-doped silane has better barrier properties compared to the control coating. Their results also showed that there was a critical concentration of cerium nitrate in the coating to obtain the optimum barrier properties for the coating.

Montemor et al. [9] evaluated corrosion behavior of hot-dipped galvanized steel pretreated with SiO_2 microparticle modified bis-1,2-[triethoxysilyl]ethane silane and bis-[triethoxysilylpropyl]tetrasulfide in an NaCl solution using impedance spectroscopy, polarization, and scanning vibrating electrode techniques. They characterized the film using X-ray photoelectron spectroscopy, Auger electron spectroscopy, and atomic force microscopy and found that bis-silane films modified with microparticles of SiO_2 are effective pretreatments for the corrosion protection of galvanized steel substrates.

Deflorian et al. [10] reported corrosion properties on copper and aluminum alloys pretreated with 3-glycidoxypropyltrimethoxysilane followed by a powder coating of epoxy-polyester. They compared the results obtained on floro-zirconate and silane treated substrates and found that silane-treated substrates had better corrosion resistance than floro-zirconate treated substrates.

Flis et al. [11] studied vinyltriethoxysilane film on iron substrates. They conducted Auger electron spectroscopy, X-ray photoelectron spectroscopy, and Fourier transformation-infra-red spectroscopy on coated metals retrieved after impedance measurements in a Na_2HPO_4 solution. They found that coated substrates exposed to air displayed an improvement in protective properties as there was an increase in charge transfer resistance and a decrease in the double-layer capacitance of the coating.

Quinet et al. [12] studied hybrid solgel coatings made of dimethoxydimethylsilane, methyltriethoxysilane, and tetrapropoxyzirconium. An organic corrosion inhibitor tertachloro-p-benzoquinone was added to each coating formulation. Electrochemical impedance spectroscopy, atomic force microscopy, and glow discharge optical emission spectroscopy showed that increasing the concentration of an organic inhibitor did not provide enough corrosion protection since the inhibitor caused disorganisation of the sol-gel system; however, lowering the concentration of the inhibitor resulted in homogenous coating structures with increased corrosion inhibition characteristics.

Bexell et al. [13] studied the surface chemistry of a γ-mercaptopropyltrimethoxysilane pretreatment followed by the application of paint on a hot-dip galvanized cold-rolled steel. They noted that with higher silane concentrations, the resultant thicker films had more cracks. Relatively thinner silane films thus were effective adhesion promoters for paint.

Wu et al. [14] studied the thermal stability and corrosion resistance of solgel hybrid coatings obtained by reacting α,ω-aminopropylpolydimethylsiloxane, 3-glicidoxypropyltrimethoxysilane, and tetraethoxysilane. Their results indicated that the thermal stability of polydimethylsiloxane-cured tetraethoxysilane coatings was lower than 3-glicidoxypropyltrimethoxysilane-cured tetraethoxysilane coatings probably due to higher thermal conductivity of silica that enhanced aliphatic n-propyl segmental degradation.

Zhang et al. [15] developed an inorganic-organic solgel derived from a SiO_2 matrix composite by reacting tetraethoxysilane and 3-(methacryloxypropyl)-trimethoxysilane in an acidic solution. They found that the thermal stability of the hybrid was enhanced with the increase in the 3-(methacryloxypropyl)-trimethoxysilane concentration in the coating formulation; and that upon heating polymerization occurred at approximately 150^{o}C followed by a complete conversion to silica at 500^{o}C.

MATERIALS AND METHODS

Materials

This section provides details about the material and experimental techniques used during the development of "SiloXel" (HCLCoat11.3) coating. Materials used in these studies were directly purchased from the manufacturer and were used without further purification, unless otherwise indicated. The following materials were used in the development of the coatings: silane-I (purity 95%) and silane-II (purity 99%) purchased from Fluka; silane-III (purity 97%) and diethyl ether purchased from Across; titanium alkoxide (purity 99%), isopropanol (purity 99.7%), and tin-based catalyst (purity 95%) purchased from Alfa-Aesar; and cerium and sodium salts, purchased from Merck.

Development of Coating: Calculated quantities of three different silanes were added to a reaction vessel and sonicated long enough to ensure proper mixing (proprietary mixture). Isopropanol was added to this mixture. In a second reaction vessel, a calculated quantity of titaniumalkoxide was added dropwise to a known amount of ultrapure water. The water was constantly stirred while titaniumalkoxide was added and then stirred again for 2 hrs. In a third reaction vessel, a calculated quantity of sodium salt was dissolved in a known amount of water and isopropanol. A known quantity of isopropanol, diethyl ether, and tin catalyst were mixed in a separate vessel.

Solutions of all four containers were mixed systematically to produce a colourless liquid that could be diluted with organic solvents to produce a series of coated samples with various thicknesses.

Surface preparation and coating of metal coupons: Metal specimens of three different sizes were used to study the barrier properties of the coatings against corrosive environments. For most of the studies, 2 in. x 2 in. coupons were used, while for atomic force microscopy observations 1 cm x 1 cm specimens were used. Coated coupons 1 in. x 1 in. were used to test the mechanical properties of the coatings. The following steps were taken for surface preparation, cleaning, and coating:

Step 1: Surface roughening of the coupons with a silicon carbide grinding paper (320 grit).
Step 2: Immersing coupons in a dilute basic solution for 1 min.
Step 3: Washing coupons in nanopure water
Step 4: Drying the coupons with compressed air
Step 5: Dip coating the coupons

All of the coated coupons were air-dried overnight and then heated to 60^{o}C for 6 hrs with the exception of coupons used for immersion testing that were cured for 15 days at 60^{o}C. These coated coupons were then stored in a dry box (McDry) at 2% RH until required for further experiments. Finally, the surface of each coupon was scanned using an Atlas Video Image Enhanced Evaluation of Weathering (VIEEW) surface analyzer.

Electrolyte Preparation: A 3.15 wt.% NaCl solution was prepared using reagent-grade chemicals and ultrapure 18 MΩ•cm resistivity water. Harrison's solution was prepared by adding 3.5 wt.% ammonium sulfate and 0.5 wt.% sodium chloride to ultrapure water. The Harrison's solution was diluted to 10% strength for the corrosion experiments.

Methods

Structural Characterization by Fourier Transform Infrared (FTIR) Analysis: FTIR spectra were measured using a Thermoelectron Nicolet™ model 720X instrument, employing liquid, gel, and solid coatings on a KBr pellet. The spectra were recorded and analyzed using the Thermo Electron Omnic® software. A blank background spectrum was collected prior to collecting a spectrum of the sample. A minimum of 60 scans of specimen were employed for each spectrum. A thin film of each liquid sample to be analyzed was spread directly on the KBr pellet and scanned in FTIR. Continuous spectra were recorded at various time intervals to monitor the hardening profile and the reaction species formed during various phases of the conversion/curing process.

Structural Verification by Raman Analysis: Raman spectra were recorded on a Thermoelectron Nicolet™ Almega™ XR dispersive Raman spectrometer. Spectra of the desired region were acquired using the

Atlus microscope and Omnic® software. Metal coupons coated with the developed coatings were analyzed directly under a dispersive Raman spectrophotometer using an integrated Atlus optical microscope Different equipment parameters such as the wavelength of the laser (785 or 532nm), laser power, resolution, and aperture (either slit or pinhole) were modulated using Omnic® Almega™ software until a true signal was observed. The optimal conditions for these experiments used the 532nm wavelength, laser power of 80%, 50µm pinhole aperture, and low sensor resolution. A background spectrum was collected prior to collecting a spectrum of the sample.

Scanning Electron Microscope (SEM) Analysis: The coating morphology was analyzed with a Hitachi S-3400N, SEM. The samples were carbon coated to prevent charging during the SEM analyses.

Atomic Force Microscopy (AFM) Analysis: AFM analysis was performed on cured samples under ambient air conditions using a Nanoscope IIIa, Digital Multimode AFM (Digital Instrument, CA), which operates in either a tapping mode or a contact mode, employing a sharp silicon cantilever. Images were collected over a wide scanning range from 250 nm to 100 µm that depended on the size of structural features present.

Nanoindentation Experiments: Nanoindentation and scratch tests were conducted using a MTS Nanoindenter® XP with a Berkovich diamond tip. Test samples were mounted with epoxy resin onto an aluminum stub. Hardness was measured using the continuous stiffness measurement option. Fused silica was used as a standard calibration sample. During the scratch tests, the platform holding the specimen was moved to create the scratch, while the indentation head controlled the load applied to the indenter. Experimental parameters were chosen as follows: scratch speed, 10 µm/s; scratch length, 500 µm; maximum lateral force, 250 mN (all orientations); maximum lateral force resolution, 2 µN; maximum normal force, 300 mN; noise level, 300 µN (without contact); and lateral force scratch orientation was with the Berkovich face forward.

Thermal Analysis: Thermogravimetric analysis was conducted on Thermo Versatherm-HS™ equipment. Liquid samples were placed in a reaction pan and the sample weight was allowed to stabilize. The scan was conducted by increasing the temperature slowly at the rate of 10 ^{o}C/min. until it reached 1000 ^{o}C in flowing air or nitrogen atmosphere.

Evaluation of the Coating

Outdoor Exposure and Corrosion Studies: Each 6061Al-T6, 2024Al-T6, and 7075Al-T6 coupon (2 in. x 2 in.) was stamped with a numeric code using a Telesis Benchmark 320 pin stamping system. Coupons were then surface treated and coated as per the set procedure. After curing, each coupon was mounted on a test rack as shown in Figure 1.

Coated metal specimens were exposed to the high-altitude Mauna Loa test site on the Big Island, which was established by the Hawaii Corrosion Laboratory, University of Hawai'i. Three sets of one bare, two coated, and one coated and scribed coupons for each aluminum alloy were exposed at the Mauna Loa test site (Figure 1). The coupons were retrieved after 2 months from the Mauna Loa test site.

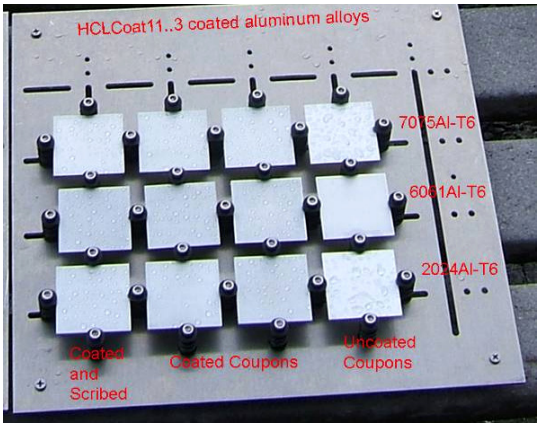


FIGURE 1- Arrangement of the SiloXel (HCLCoat11.3) coated coupons on a test rack at the Mauna Loa test site.

Immersion Test: Coupons of three different aluminum alloys (i.e. 2024Al-T6, 6061Al-T6 and 7075Al-T6) were coated with the developed coatings and allowed to harden for 15 days at 60^{o}C. Coupons were installed in acrylic holders and placed in glass beakers. Each beaker contained three coupons. The beakers were then filled to the same level (500 ml mark) with electrolyte. The beakers were covered and placed in a 30 ^{o}C constant-temperature bath for 30 days. After the designated exposure time passed, the coupons were retrieved and washed with ultrapure water and then air dried.

Accelerated Weather Corrosion Test: Coated aluminum coupons were mounted on a plastic rack and exposed to an accelerated weather environment in a Singleton CCT-10 Cyclic Corrosion Test Chamber. The test was conducted as per GM9540P standards

UV Exposure Test: First, each unexposed coated coupon was scanned using a VIEEW image analyzer. Then the coupons were mounted on an aluminum rack and exposed in a Q-Panel Lab Products Q-Sun XE3 Xenon Arc Test Chamber (Q-Sun). UV Exposures occurred for 6 hrs a day for 10 days. The back panel temperature of the chamber was maintained at 70^{o}C; the chamber air temperature was 47^{o}C and the relative humidity was 50%. Sample locations in the chamber were rotated every day to ensure a nominally even exposure to all coupons. The total amount of UV light energy that fell on each sample in 60 hrs. was 119.0 KJ/m^{2}.

VIEEW Analysis: Coated and uncoated coupon surfaces were scanned before and after their respective exposures using a VIEEW digital image analyzer from Atlas Electric Devices Company. VIEEW equipment is capable of capturing digital images of samples under various lighting schemes optimized to highlight and enhance surface defects to digitally process images, in order to measure and count defects with a comprehensive statistical profile. The VIEEW equipment incorporates two different illumination methods: (1) diffuse, chromatic (color) lighting for the detection of variations in chromatic contrast; and (2) direct lighting to measure variations in geometric reflection (gloss) and its textural characteristics. The area under the scan was selected and lights for the reflection were optimized using Atlas imaging software. During the sample topology analysis, only light reflected from the surface of the clear coating, not from the deeper pigmentation layer is analyzed. Red color on the scans indicates the corroded or damaged area.

RESULTS AND DISCUSSION

Structural Verification with FTIR Spectroscopy

FTIR spectra were recorded at the gel and solid stages of the SiloXel precursor. Line spectra shown in Figure 2 indicated that the amount of hydrocarbon in the coating was low in the coating composition. The two weak peaks appearing at 2922cm^{-1} and 2971cm^{-1} corresponded to symmetric and asymmetric –CH_2 bond stretching modes present on the silicone moiety. The presence of this hydrocarbon unit reveals the planarization characteristic of the coating macromolecular chains.

A hump at 3400cm^{-1} indicated the presence of hydrogen bonding in the molecular structure. The strong, sharp peak at 1271cm^{-1} was due to Si-CH_3 vibrations. The peak at approximately 1100cm^{-1} was due to Si-O-Si vibrations. The peak at 911cm^{-1} was due to an –OH group produced as a result of the hydrolysis of alkoxysilanes. Note that the peak at 911cm^{-1} was stronger in the gel stage but weaker in the solid stage, probably due to the consumption of the generated hydroxyl groups during the crosslinking and hardening processes. Another strong peak at 777cm^{-1} was likely due to the contribution from hydrocarbons in the ceramic structure.

Figure 3 shows the 3D spectra recorded as a function of time and temperature. The liquid precursor to coating was heated at a constant rate of 10^{o}C/min. Gases eluting from the compound, with the rise in temperature, were continuously monitored and recorded by an integrated FTIR system. It can be seen that most of the volatile components (mostly solvents) eluted up to 100^{o}C. Only a small amount of CO_2 (~2450cm^{-1}) was found eluting until the end of the experiment. Appearance of CO_2 in the spectra indicated that a methyl group was actively involved during the cerametization of the silicones.

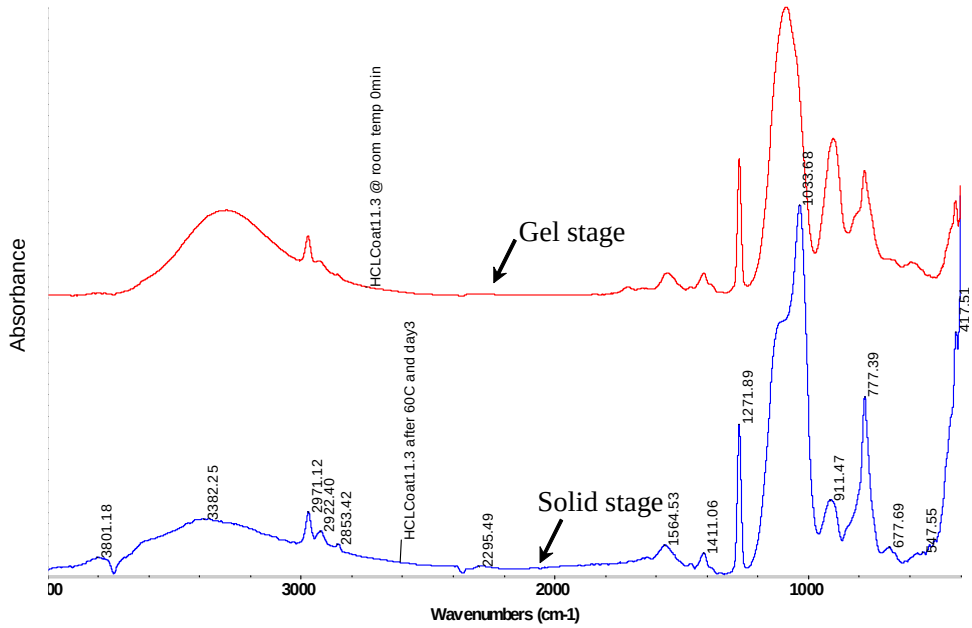


FIGURE 2- Gel stage and solid state FTIR analyses of SiloXel (HCLCoat11.3) precursor and film.

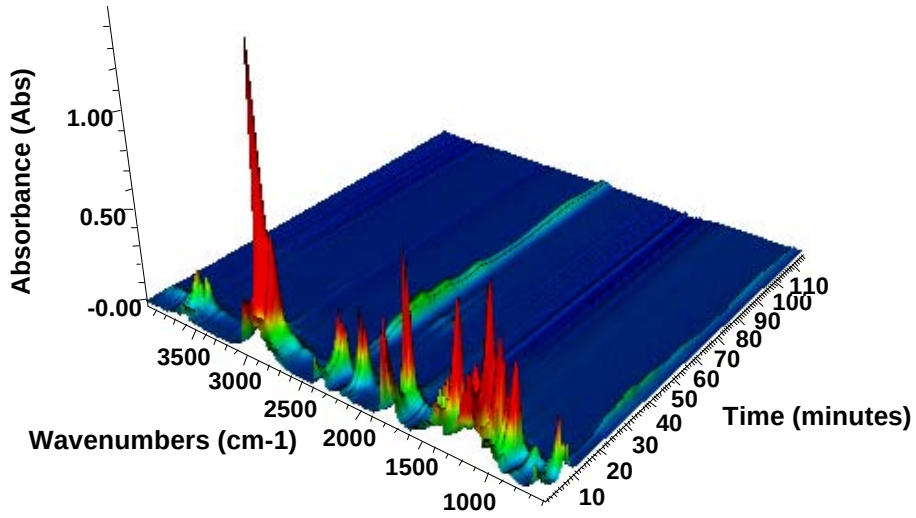


FIGURE 3- FTIR analysis of SiloXel precursor as a function of time and temperature. The heating rate for this pyrolysis experiment was 10^{o}C/min.

Structural Confirmation by Raman spectroscopy

Raman spectroscopy is useful for the determination of organic as well as inorganic components in a chemical structure. In the solid state (Figure 4), the SiloXel coating showed five distinct peaks between 450cm^{-1} and 3000cm^{-1}. Two sharp peaks appearing at 2963cm^{-1} and 2902cm^{-1} corresponded to the symmetric and asymmetric –CH_2 hydrocarbon portion of the spectra. The relatively weak peak at 1401cm^{-1} corresponded to some form of hydrocarbon. Another weak peak at 780cm^{-1} indicated the possible presence of oxygen as –OH functionality. The peak appearing at 456cm^{-1} corresponded to the elemental form of silicon.

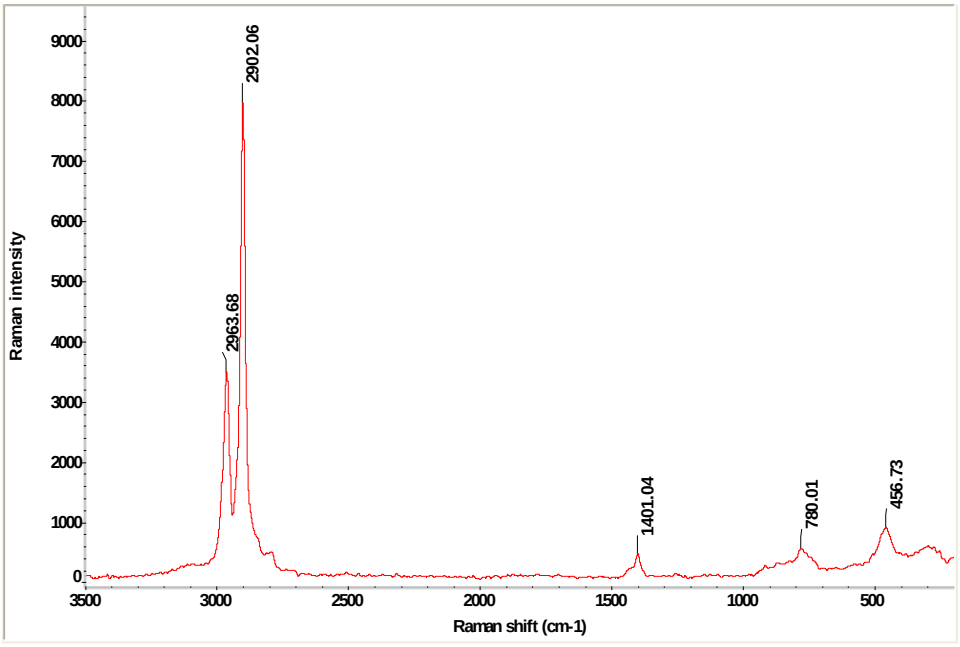


FIGURE 4- Solid state Raman spectroscopic analysis of SiloXel coating.

Surface Morphological Studies by SEM Technique

Surface morphology of the coating was investigated using the SEM technique (Figure 5). It was found that the coating had a dense structure with a uniform distribution of hillocks on the surface. We believe that origin of these hillocks on the surface coating were due to self assembly of the macromolecular structures during the hardening process. There was no sign of cavities, pin holes, or any other type of surface defects. The thickness of the matrix coating was approximately 2 µm as estimated by the SEM of a scratched coated surface (not shown here).

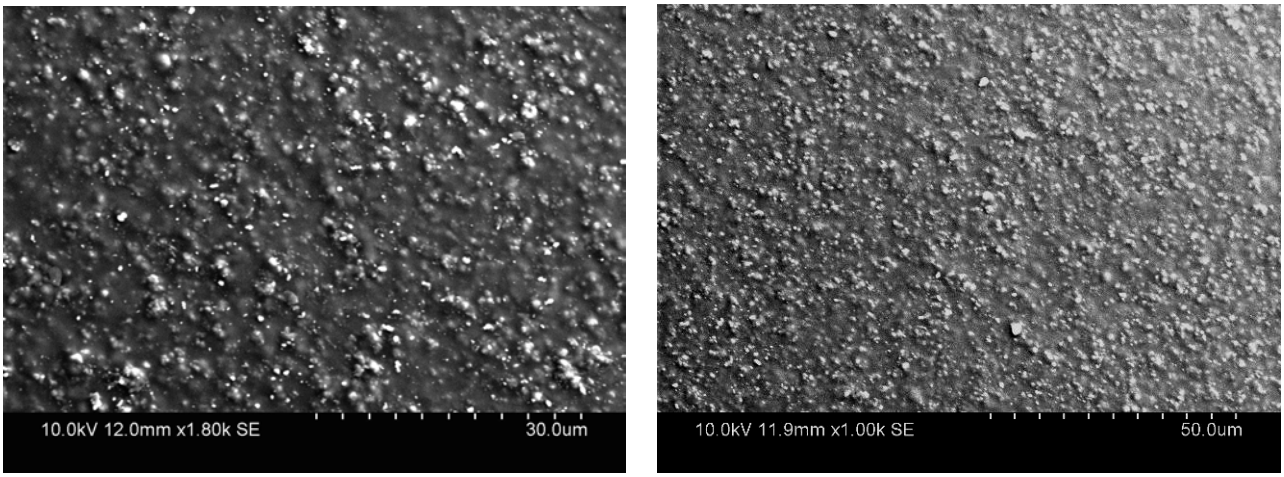


FIGURE 5- SEM images of dense SiloXel coating on 6061Al-T6 substrate. Micrographs were taken at two different magnifications for the broader and concentrated view.

Surface Morphology through AFM Analysis

AFM analysis of the SiloXel coating has shown (Figure 6) that surface roughness of the coating was in the nanometer regime. There was no sign of pinholes or cavities on the thin solid film, suggesting that the solid coating film obtained after the complete hardening profile consisted of densely packed 3D network structures. The surface roughness appearing at nanometer dimensions could be due to the roughness associated with the metal substrate surface.

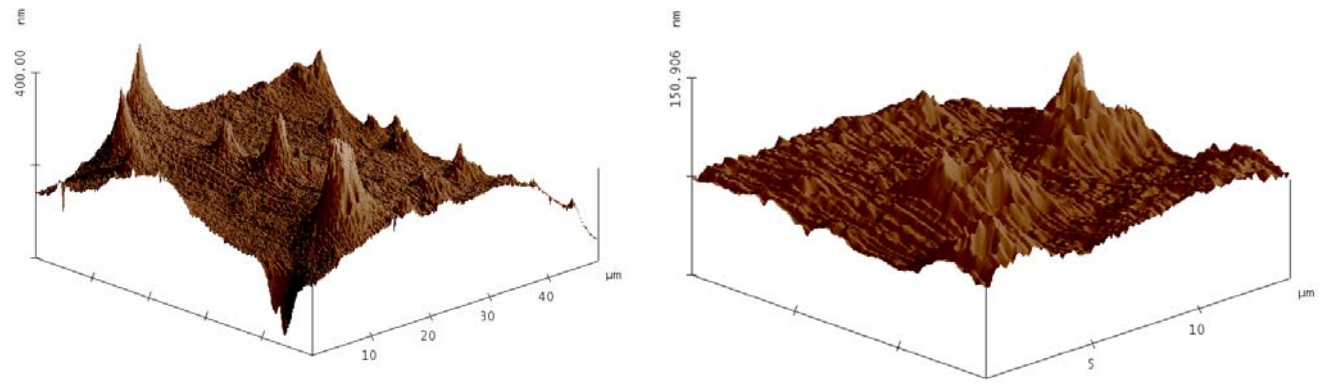


FIGURE 6- Atomic force nanoscopic image of dense SiloXel coating on 6061Al-T6 substrate. The nanograph supports the formation of dense ceramic like structure in the solid coating. Wave like patterns observed in nanographs are appearing due to the scratches on the surface of the substrate. These scratches can cause minor effect in surface topography but they are much smaller than the hillocks dimensions.

Inert and Oxidative Atmosphere Thermogravimetric Analysis

Thermal analysis shown in Figure 7 was conducted on the precursor solution that contained large amounts of volatile solvent. Parameters reported here (Table 1) were derived by assuming that most of the solvent had evaporated before reaching 100^{o}C, so it was not included in the decomposition calculations of the coating's solid content. After all the volatile components are lost, the precursor transforms to a solid mass and decomposes in the subsequent heating steps as the temperature is increased.

Here $D_{0.1}$ represents the temperature for 10% decomposition of the solid coating while $D_{0.5}$ indicates temperature at which half of the solid content of the coating decomposes. MRDT is the temperature for the maximum rate of decomposition of the solid coating.

In an inert-atmosphere condition, the precursor to coating decomposed by the 10% at 109^{o}C but retained half of its initial solid content at 252^{o}C. In the oxidative case, the SiloXel coating decomposed by 10% at 112^{o}C, while the temperature for 50% decomposition was 358^{o}C. The maximum rate of decomposition occurred at 300^{o}C in an inert atmosphere, while in an oxidizing environment it occurred at 200^{o}C. Higher thermal stability in the oxidative atmosphere is probably due to the formation of silicon dioxide. Residue content obtained after the complete decomposition was similar in both atmospheres.

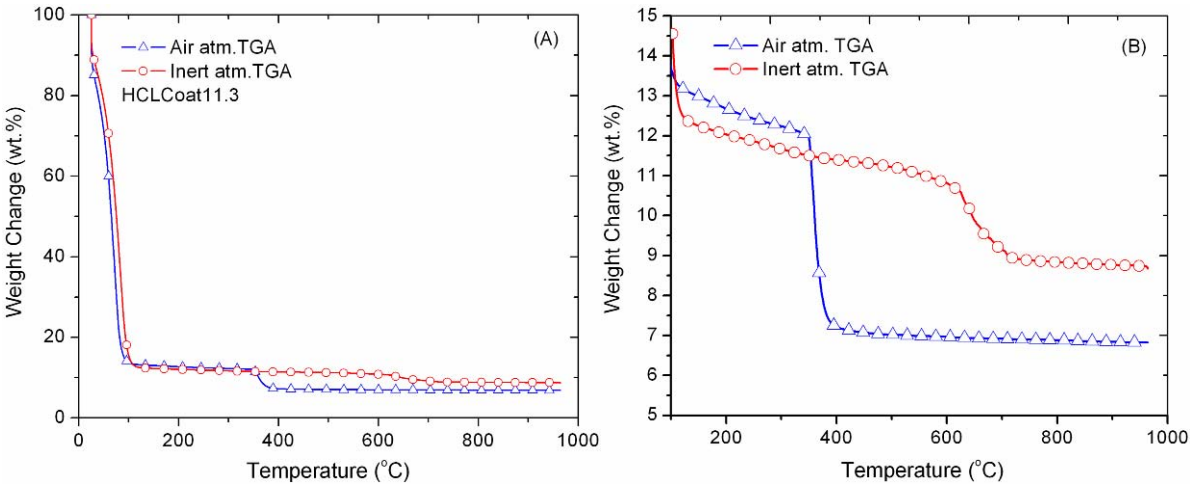


FIGURE 7- Inert and oxidative atmosphere thermogravimetric analysis of SiloXel (HCLCoat11.3) coating precursor (A). Zoomed-in view of the coating-precursor initial and final decomposition pattern (B).

TABLE 1
INERT AND OXIDATIVE ATMOSPHERE PARAMETER OF SiloXel COATING

Coating	Inert atmosphere parameters				Oxidative atmosphere parameters			
	$D_{0.1}$ (°C)	$D_{0.5}$ (°C)	MRDT (°C)	Residue (%)	$D_{0.1}$ (°C)	$D_{0.5}$ (°C)	MRDT (°C)	Residue (%)
SiloXel	109	252	300	58	112	358	200	52

Nanomechanical Analysis of Coating on Three Different Substrates

Three aluminum alloys were coated with SiloXel and hardened. These test coupons were subjected to nanoindentation experiments (Figure 8). The hardness and modulus of the coating on the 6061Al and 7075Al substrates were similar through the penetration depth of 350 nm, suggesting that the substrate adhesion and hardening mechanisms were identical. The strength and modulus trends of the coating on 2024Al were similar to those on the 6061Al and 7075Al substrates, but only up to a penetration depth of approximately 50 nm. Above this depth of penetration, the strength and modulus for the coating on 2024Al increased at a greater rate than those on the other substrates. Further research is required to determine why the strength and modulus increased. It is not known if this is purely a substrate effect or if it is related to a reaction between the coating and the substrate during the curing process. The 2024Al alloy (max 4.9 wt% Cu) has significantly more copper than that of 6061Al (max 0.4 wt% Cu) and 7075Al (max 2.0 wt% Cu) which could result in more substrate corrosion on 2024Al during the curing process.

TABLE 2
NANOMECHANICAL ANALYSIS VALUES OF SiloXel COATING

Test	Modulus-Avg Over Defined Range	Hardness-Avg Over Defined Range	Peak Load	Peak Hardness	Elasticity Ratio	Modulus From Unload	Hardness From Unload
	GPa	GPa	mN	GPa		GPa	GPa
2024Al	5.913	0.237	1.198	0.517	0.293	25.77	0.486
6061Al	4.887	0.346	0.749	0.406	0.867	4.896	0.480
7075Al	4.769	0.310	0.658	0.357	0.842	4.367	0.396

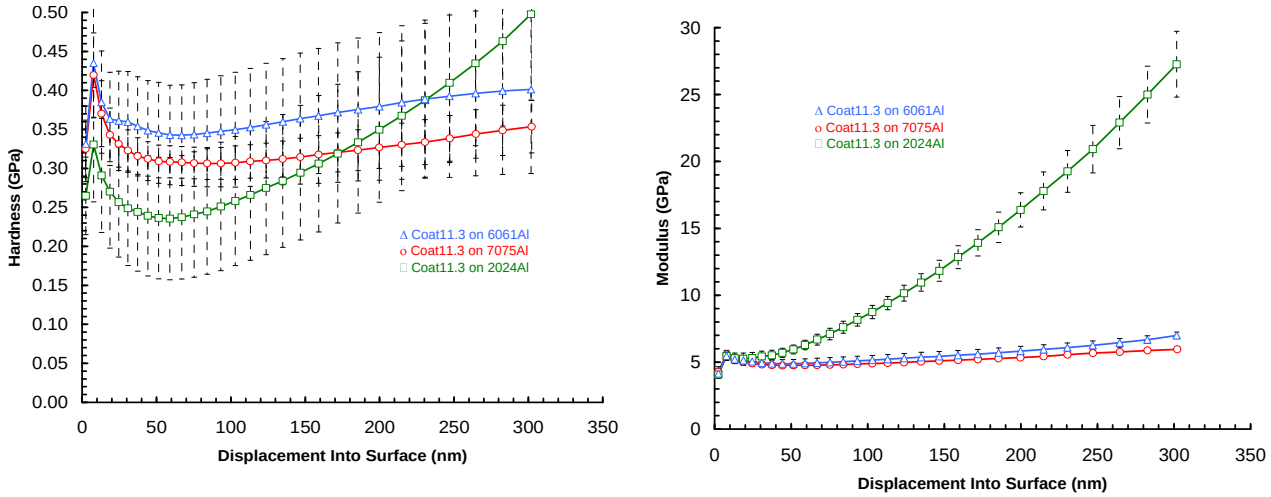


FIGURE 8- Nanomechanical hardness and modulus of SiloXel (HCLCoat11.3) hardened on three different aluminum alloys. The data is an average of 6 runs. Standard deviation bars are also plotted.

In-lab UV-Radiation Exposure of the Coated Coupons

A set of nine coated coupons of three different aluminum alloys were exposed to the UV chamber for 60 hrs. Figure 9 shows a VIEEW scan of coated coupons before and after the exposure. No visible damage was observed on the coated surface after the UV chamber exposure period. Raman spectra were also recorded before and after exposure, and no distinct changes were observed in the spectra (Figure 11). The coupons were immersed in 10% Harrison's solution for 30 days to assess if the UV exposure compromised the barrier properties of the coating. Results from the immersion experiments are discussed in a following section.

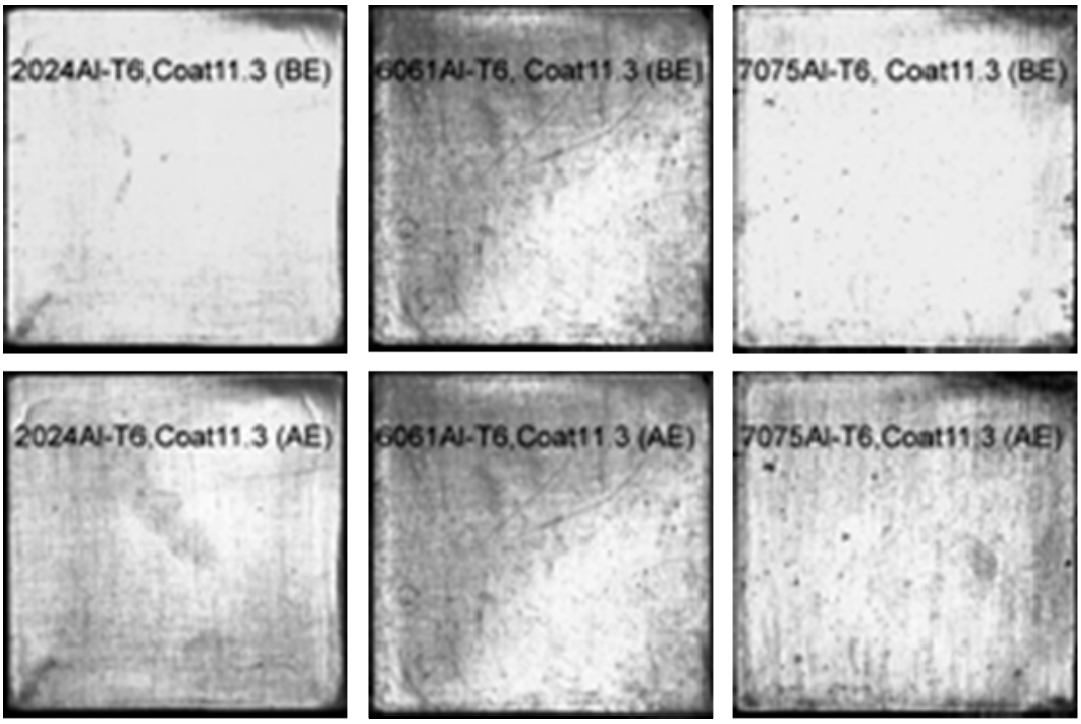


FIGURE **9**- VIEEW scans of coupons before (BE) and after (AE) exposure to UV radiation for 60 hrs. No visible damage was found on the coated surface.

Evaluation of Coatings after Outdoor Exposure to a UV-Radiation Test Site

A high-altitude Mauna Loa (MLO) test site in Hawaii which receives high levels of solar radiation was chosen for natural solar radiation testing. Coated coupons of the three different aluminum alloys were scanned using the VIEEW instrument before exposure at the test site. Coupons were retrieved after 4 months of exposure and scanned again using the VIEEW instrument. No visual damage was observed after the 4-month exposure (Figure 10).

Raman spectra were also recorded before and after exposure (Figure 11). Changes in the Raman spectra (Figure 11) indicated structural changes in the coating possibly due to degradation of the coating or to extended reactions occurring between different chemical entities in the coating. The implications of these spectral results are still under investigation.

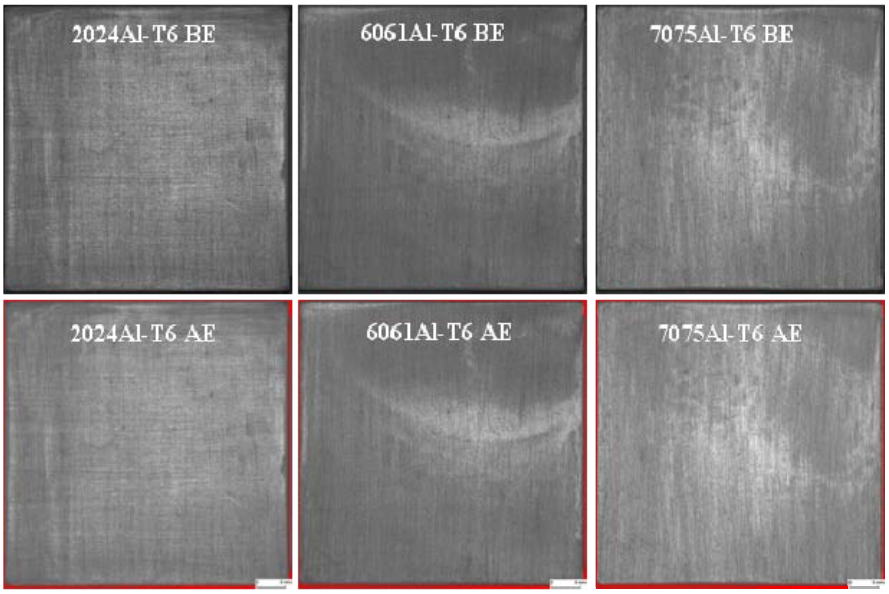


FIGURE 10- VIEEW scans of coupons before exposure and after exposure to UV radiation for 4 months at an outdoor site in Mauna Loa, Hawaii. No visible damage was found on the coated surface.

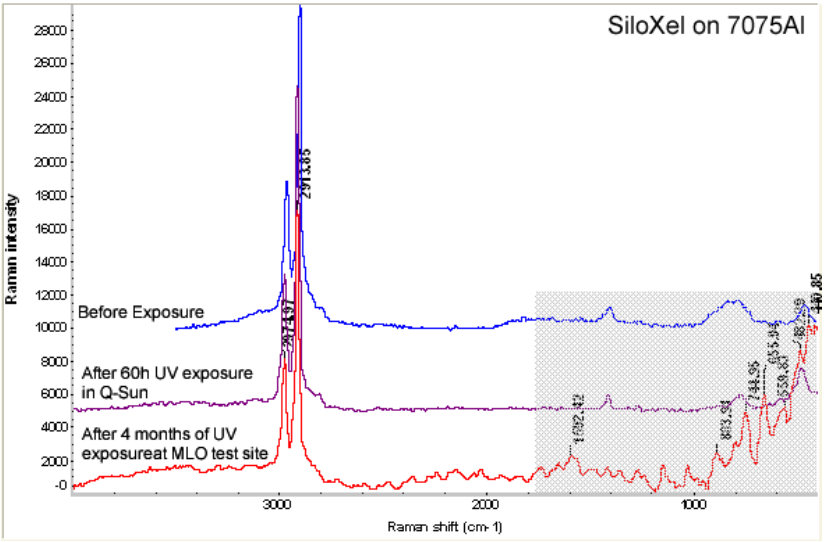


FIGURE 11- Raman spectra patterns of SiloXel (HCLCoat11.3) coated on a 7075Al substrate before and after exposure to laboratory-generated and aggressive outdoor solar radiation at MLO. Similar results were observed for coated 6061Al and 2024Al specimens.

Immersion Experiments in 10% Harrison's Solution

A set of nine coated coupons and three uncoated coupons were exposed in the Q-Sun for 60 hrs to observe the effect of UV light on the coatings. Six out of nine coupons were used for subsequent immersion testing along with the three uncoated coupons. Another set of six coated coupons that were not exposed to UV light were also selected for this test. A 10 wt% Harrison's solution was used as the electrolyte. Both the coated and uncoated coupons were immersed in the corrosive solution and retrieved after 30 days of immersion. Coupons were then washed with ultrapure water and air dried, at which point they were subjected to surface analysis employing the VIEEW surface analyzer.

It was expected that the UV-exposed coated coupons immersed in the electrolyte would show evidence of corrosion. On the contrary, there were no signs of corrosion, suggesting that the SiloXel coating acted as an impervious coating under immersion conditions even after UV exposure. Surface damage of the coupons was analyzed using VIEEW (Figure 12). Each coupon was labeled with the aluminum alloy type and whether it was coated (C) or uncoated (Ba), exposed to UV radiation (E) or unexposed to UV radiation (UE).

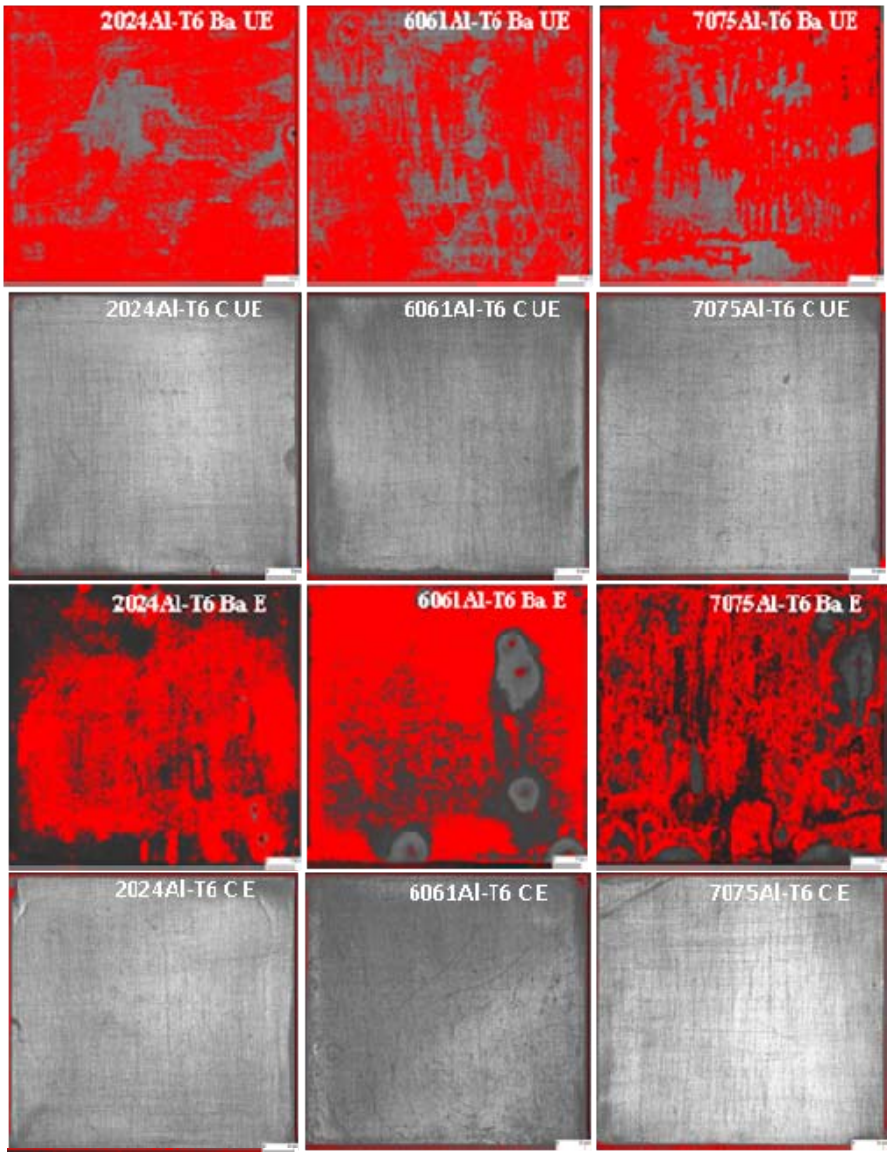


FIGURE 12- VIEEW images of coupons retrieved after 30 days of immersion experiment in 10% Harrison's solution. Uncoated coupons (Ba) suffered severe corrosion while coated coupons (C) remained unaffected. Both exposed to UV radiation (E) and unexposed to UV radiation (UE) coupons were immersed in corrosive media.

Immersion Experiments in 3.15wt.% NaCl Solution

A set of three coupons of three aluminum alloys were coated and immersed in 3.15 wt% NaCl solution for 30 days. Uncoated coupons of the same aluminum alloys were also immersed simultaneously for comparison. Figure 13 shows VIEEW analysis of coated (C) and uncoated (UC) coupons retrieved after 30 days of immersion.

Uncoated coupons suffered severe surface damage due to corrosion, while the coated coupons were not affected. Slight corrosion at the edges of the coated coupons was probably due to edge defects in the coating during the dip-coating process.

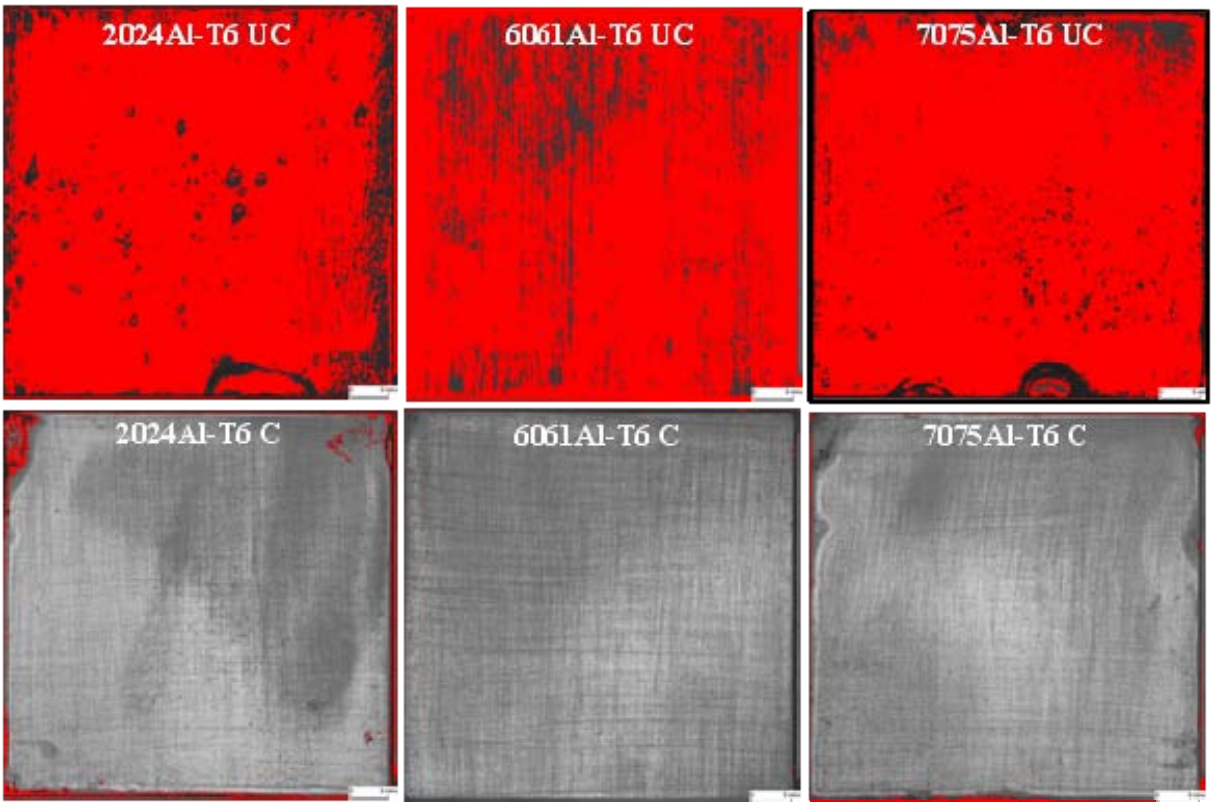


FIGURE 13- VIEEW images of coupons retrieved after 30 days of immersion in 3.15wt.% NaCl solution. Uncoated coupons (UC) suffered severe corrosion while coated coupons (C) remained relatively unaffected.

Results from Cyclic Corrosion Test Chamber Experiment (CCTC)

Figure 14 shows VIEEW analysis of coated and uncoated coupons exposed in a cyclic corrosion test chamber in accelerated and simulated corrosive conditions. The test was done as per the GM9540P standards. The three types of aluminum alloy coupons were coated and exposed in the cyclic corrosion test chamber for 8 days. One coated coupon from each set was scribed to study the effect of corrosion at a deliberate coating defect. For comparative purposes, uncoated coupons of the same aluminum alloys were exposed simultaneously.

The uncoated coupons suffered severe surface damage due to corrosion, while coated coupons were not affected. Slight corrosion at the edges of the coated coupons was probably due to edge defects. Scribed coated coupons corroded in the scratch area, but there was no sign of coating lift-off adjacent to these scribed sites.

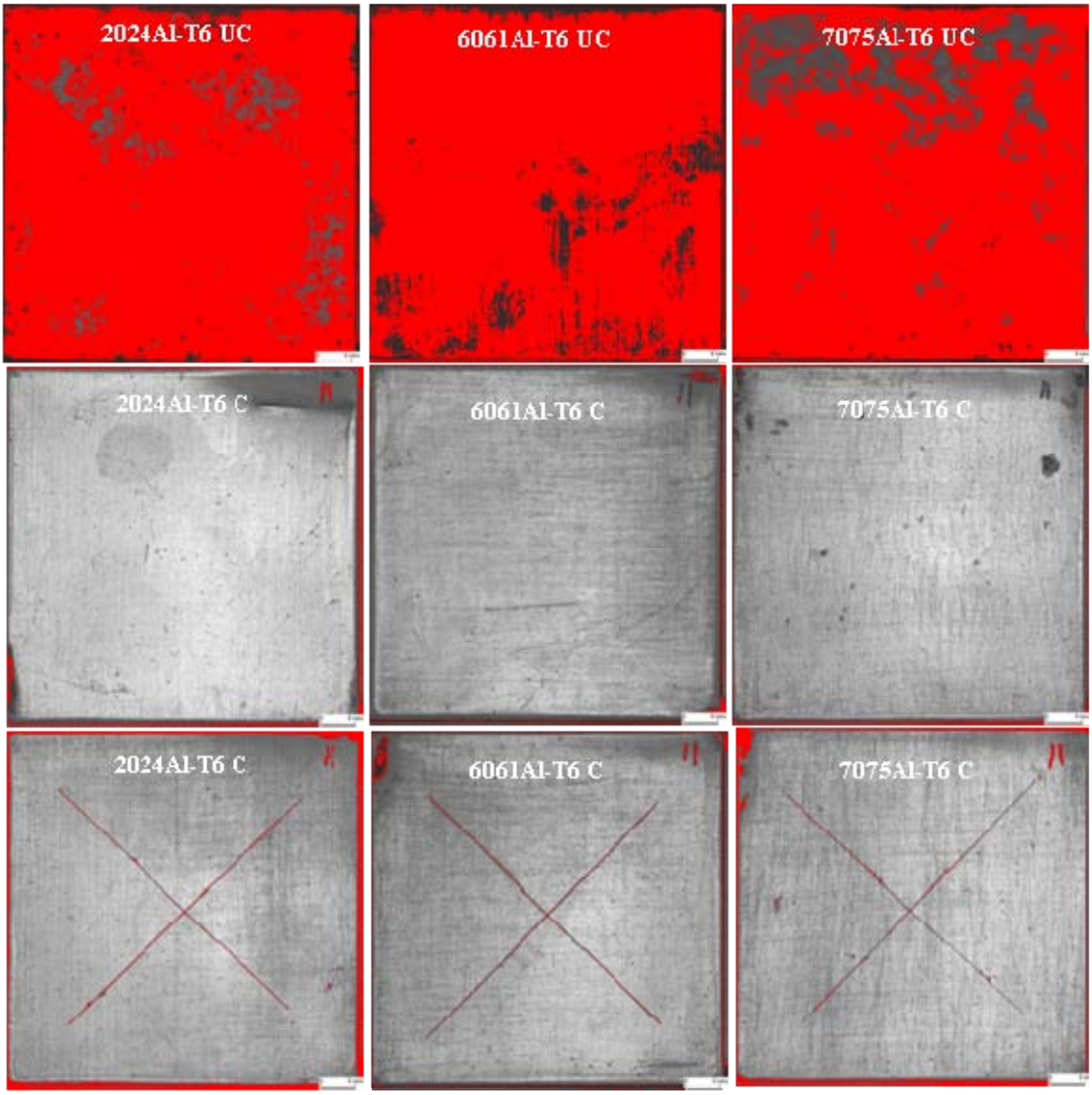


FIGURE 14- VIEEW images of coupons retrieved after 8 days of the CCTC experiment. No corrosion was seen on the coated metals away from the scribe.

Morphological Analysis of Coated Coupons after Exposure to Corrosive Media

Coated specimens were immersed in 3.15 wt.% NaCl solution for 30 and 90 days. Surface morphology was recorded before and after the immersion experiment to monitor any corrosive activity on the coated surface. Samples were periodically removed from the immersion bath to examine the degree of corrosion on the coated substrates. In the case of coated 2024Al-T6 specimens, precipitation of salt or corrosion-like activity was seen after 30 days of immersion, while the coated 7075Al-T6 specimens had few corroded regions even after 90 days of immersion. No corrosion or surface degradation was seen on the coated 6061Al-T6 test specimens after 90 days of immersion. Figure 15 shows AFM images of coated specimens after being retrieved from the immersion experiments. Several dark spots were seen on the 7075Al-T6 coated specimens (2D image) corresponding to possible corrosion sites. In case of the 2024Al-T6 specimens (3D image), corrosion product accumulated, forming elevated regions.

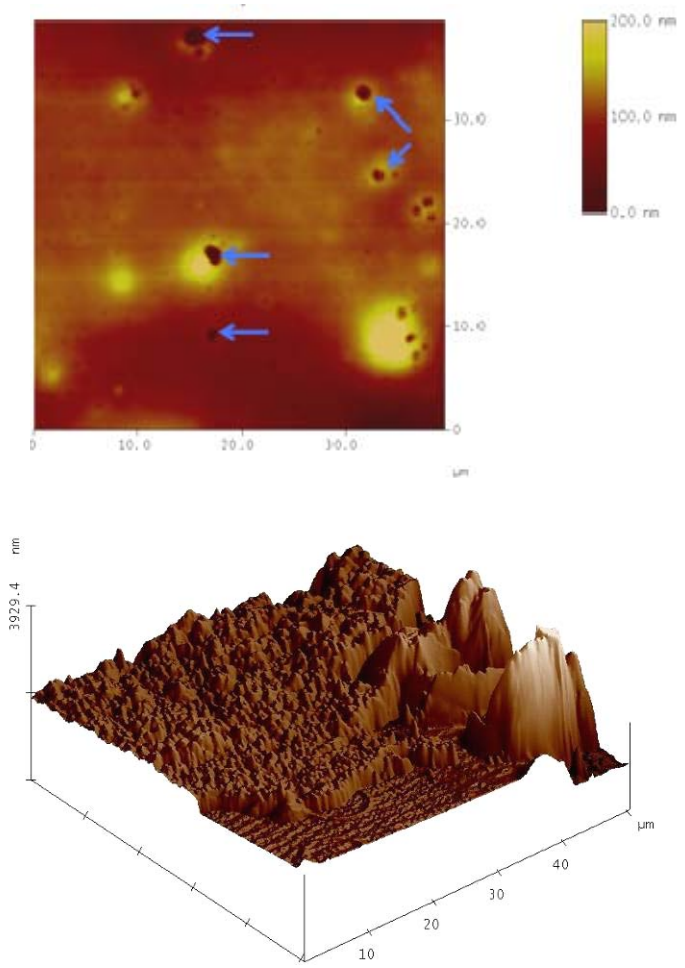


FIGURE 15- 2D AFM images of 7075Al-T6 coated test specimen retrieved after 90 days (top) and 3D topography of coated 2024Al-T6 after 30 days of immersion in 3.15wt.% NaCl solution (bottom).

CONCLUSION

SiloXel, a high-silicon content impervious coating, was developed by mixing four different chemical components. Three different aluminum substrates—2024Al-T6, 6061Al-T6, and 7075Al-T6—were coated with SiloXel and tested in different corrosive environments.

FTIR and Raman analysis confirmed low concentration of hydrocarbons and high concentration of silicone in the coating structure. It was also found from thermogravimetric and FTIR analyses that most of the hydrocarbon decomposes and elutes as CO_2 and hydrogen gas on elevated-temperature heating. Thermal properties of the liquid precursor of the coating were analyzed in inert and oxidative atmospheres using a thermogravimetric analyzer. Thermal stability of the coating was found to be higher in the oxidative atmosphere than in the inert atmosphere, probably due to the formation of silicon dioxide.

Surface morphology and inherent microstructural details were studied using the SEM that revealed a highly-dense coating structure without pinholes and cavities. The estimated thickness of the coating was approximately 2 µm.

The mechanical properties of the coating were also examined using a nanoindentation technique. It was found that the hardness of the coating on the different aluminum substrates was comparable.

The SiloXel coating showed good resistance to 60 hrs of high intensity UV radiation in a xenon arc weathering test chamber. No visual surface damage or changes in the Raman spectra were detected after the exposure period. To investigate the effect of UV radiation on the barrier properties of the coating, coupons retrieved after UV radiation exposure were also subjected to subsequent immersion testing for 30 days in 10% Harrison's solution. No corrosion damage was seen on the UV-exposed coated coupons, suggesting that the coating remained intact even at the molecular level. Accordingly, non-UV exposed coated specimens were also unaffected by the 10% Harrison's solution.

The coated aluminum alloys were also exposed at a high-altitude test site on Mauna Loa, Hawaii, for natural solar radiation exposure. After a long-term 4-month exposure, no visual coating defects were found, but there were some changes in the Raman spectra, which needs to be investigated further.

Immersion experiments in 3.15wt.% NaCl solution were also conducted on the coated aluminum alloys to further evaluate the barrier properties of the coating. No corrosion was observed after 30 days of exposure except for slight corrosion at the edges and corners of some coupons.

The coated aluminum alloys were also subjected to 8 days of accelerated corrosion (GM9540P). Uncoated coupons suffered severe corrosion, the coated coupons showed little or no corrosion, and coated and scribed coupons only showed corrosion at the scribe with no evidence of coating lift-off.

Changes in surface morphology before and after the corrosion experiments were studied using the AFM. After a long exposure periods of 30 and 90 days in 3.15 wt% NaCl, slight evidence of corrosion was observed on the 2024Al-T6 and 7075Al-T6 alloys but not on the coated 6061Al-T6 alloy.

In short, the SiloXel coating imparted excellent corrosion resistance to the aluminum alloys and has potential to be used as an effective barrier in aggressive environments.

Future research includes examination of the coating in various environments including marine, rain forest, volcanic (with acid rain), agricultural, and industrial areas.

ACKNOLEDGEMENT

The authors are grateful for support of the Pacific Rim Environmental Degradation of Materials Research Program under US Army Contract W15QKN-07-C-0002. The authors are particularly grateful to program manager Mr. Robert Zanowicz, and Mr. John Theis of the Army Corrosion Office. The authors would also like to thank Dr. Ralph P.I. Adler from Army Research Laboratory for providing valuable comments on the manuscript.

REFERENCES

1. R. Pena-Alonso, L.Tellez, J. Rubio, and F. Rubio, *J Sol-Gel Sci Tech*, **38**, 133 (2006).
2. S. Etienne-Calas, A. Diru, and P. Etienne, *J Non-Cryst Solid*, **344**, 60 (2004).
3. L. Y. L. Wu, G. H. Tan, X. T. Zeng, T. H. Li, and Z. Chen, *J Sol-Gel Sci Tech*, **38**, 85, (2006).
4. A. A. Al-Juhni and B. Z. Newby, *Prog Org Coat*, **56**, 135 (2006).
5. F. Zucchi, V. Grassi, A. Frignani, C. Monticelli, and G. Trabanelli, *Surf Coat Tech*, **200**, 4136 (2006).
6. S. A. Kumar, T. Balakrishnan, M. Alagar, and Z. Denchev, *Prog Org Coat*, **55**, 207, (2006).
7. S. M. Mirabedini, S. Pazoki, M. Esfandeh, M. Mohseni, and Z. Akbari, *Prog Org Coat*, **57**, 421 (2006).
8. W. Trabelsi, P. Cecilio, M. G. S. Ferreira, and M. F. Montemor, *Prog Org Coat*, **54**, 276 (2005).
9. M. F. Montemore, A. M. Cabral, M .L. Zheludkevich, and M. G. S. Ferreira, *Surf Coat Technol*, **200**, 2875 (2006).
10. F. Deflorian, S. Rossi, and L. Fedrizzi, *Electrochem Acta*, **51**, 6097 (2006).
11. J. Flis and M. Kanoza, *Electrochem Acta*, **51**, 2338 (2006).
12. M. Quinet, B. Neveu, V. Moutarlier, P. Audebert, and L. Ricq, *Prog Org Coat*, **58**, 46, (2007).
13. U. Bexell and T. M. Grehk, *Surf Coat Tech*, **201**, 4734 (2007).
14. K. H. Wu, C. M. Chao, T. F. Yeh, and T. C. Chang, *Surf Coat Tech*, **201**, 5782 (2007).
15. X. Zhang, Y. Wu, S. He, and D. Yang, *Surf. Coat Tech*, **201**, 6051 (2007).